



**CRASHWORTHY DESIGN OF HELICOPTER COMPOSITE  
AIRFRAME STRUCTURE**

By

Richard L. Boitnott

U.S. Army Aviation Research and Technology Activity

Hampton, Virginia USA

And

Christof Kindervater

DLR Institute for Structures and Design

Stuttgart , Germany

**FIFTEENTH EUROPEAN ROTORCRAFT FORUM**

SEPTEMBER 12 - 15, 1989 AMSTERDAM

# CRASHWORTHY DESIGN OF HELICOPTER COMPOSITE AIRFRAME STRUCTURES

by

Richard L. Boitnott  
U.S. Army Aviation Research and Technology Activity  
Langley Research Center  
Hampton, Virginia 23665-5225, U.S.A.

Christof Kindervater  
Institute for Structures and Design, DLR Stuttgart  
Pfaffenwaldring 38-40, 7000 Stuttgart 80, Germany

## Abstract

This paper will report on research conducted by the DLR and the U. S. Army under a Memorandum of Understanding (MOU) to investigate the crashworthy behavior of composite materials and generic structural elements. At the element level, energy absorption results from the static crushing of cruciforms and sine wave beams will be presented. These elements are representative of keel beam and bulkhead intersections in the subfloor of rotorcraft. At the substructure level, static and dynamic vertical crushing tests of composite frames and subfloor sections will be discussed. These test specimens which fail primarily in bending are typical of structural components used in the upper and lower portions of rotorcraft airframes.

## 1. Introduction

In 1979 a Memorandum of Understanding (MOU) on "Helicopter Flight Control" was established between the U. S. Army and F. R. G. Federal Minister of Defense (BMVg). The MOU has been expanded beyond its original scope of helicopter flight control. In 1985 a task was started to enhance existing research programs on the crashworthy behavior of composite aircraft. This "Composite Structural Crashworthiness" task focuses on understanding the crashworthy potential of composite materials and generic structural elements. A number of joint research studies at the laminate level, the element level, and the substructure level have been completed to accomplish the MOU goals.

The design requirements in MIL-STD-1290 A and ADS-36 (1 and 2)\* define survivable crash scenarios of military helicopters. Helicopter crashworthiness requires the maintenance of a protective shell around the occupants in addition to absorbing vehicle kinetic energy. Unrealistically high crash protection leads to severe weight penalties which negatively influence the velocity, range, maneuverability, operating

-----

\* Numbers in parentheses designate references at end of paper

economy and radar cross section of the rotorcraft. In the next generation of military helicopters, composite materials will be used extensively in all primary structure. A prognosis for the next 10 years is that composites will be used for up to 80 percent of the structural weight of a helicopter.

Composite materials offer considerable potential advantages over metallic materials from the perspective of weight, design flexibility and fabrication cost. The micromechanical energy absorption mechanisms of composites are quite different from those of aluminum which dissipates energy by plastic hinge formation and material yielding. Therefore, a comparison of the energy absorption performance of equivalent composite and aluminum structural elements is taken into account whenever possible. Composite rotorcraft must be designed carefully to assure crashworthiness because material systems such as graphite-epoxy fail in a brittle fashion. High energy absorption has been obtained only for compressive loadings where brittle fracturing of the composite into short sublaminates occurs during crushing (3). Cruciform and sine wave beam structural elements are examples of compressively loaded structural components in rotorcraft (4). Under tensile or bending loads structural integrity may be lost at initial fracture and energy absorption can be low. Under crash conditions aircraft structural elements experience complex loadings which are not always compressive. Previous research examining the response of composite structures to crash type loadings is limited. Composite helicopter roof frames were examined in reference 5. Loads from large overhead masses such as transmissions and rotors are generally reacted through these frames. The most severe loads applied to these frames result from the crash condition. References 6 and 7 present results for drop and crush tests on graphite-epoxy fuselage frames and floor sections. Thus, with only limited crash response information available, a need exists to examine generic composite structures under crash loadings. This paper will describe vertical crush tests of cruciform elements, sine wave beam sections and graphite-epoxy fuselage frames and floor sections. Fig. 1 describes the scope of the presented work.

## 2. Cruciform structural elements

### 2.1 Cruciform specimens

There are numerous design possibilities for improving the crushing behavior of cruciform elements. The main purpose of this paper is to summarize the crashworthy aspects of rotorcraft structural elements. Reference 4 provides details on the design criteria for the load carrying capability of the cruciforms. The "ideal" crushing characteristics of subfloor elements are discussed in reference 8. A constant or slightly increasing crushing load was determined to be "ideal" from parametric crash simulation studies using the hybrid computer code KRASH. The simplest design examined in this paper was "notching the corners" at the intersection of the keel beams and bulk heads. For the aluminum cruciforms this was performed by the "notched corner" concept having single (A1N 1) and multiple notches (A1N 2) (see Fig. 2). Also, for composite hybrid (H) cruciforms (mixture of Carbon Fiber Composite (CFC) and Aramid Fiber Composite (AFC) layers in the laminate) the multiple notch concept (HN) was used. Another "notched corner" design was the corrugated edge joint design (HW) which is also illustrated in Fig. 2. The corrugated edge joint uses a nonconventional approach to initiate local failures at the joint. Another possible way of influencing the crushing behavior of

cruciforms is through material selection. Hybridization of CFC/AFC was used mainly to improve the post crash integrity of the cruciform elements.

The cruciform labeled "improved design" variant (HTP) in Fig. 3, takes into account the experience gained from composite tubular specimen crushing. Circular or square tube sections have demonstrated high energy absorption performance (3 and 9). Therefore, the bulkhead hybrid laminates were split along their middle and bolted together with the keel beam section. This fabrication formed a tubular column-like structure in the center of the cruciform. At the bottom of both bulkhead sections a bevel trigger was provided and the edge joints were tapered from bottom to top. These load-introduction mechanisms were used to reduce the initial spike crushing loads and cause the sustained crushing force to increase slightly with increasing deflection.

All cruciform elements were quasi-statically crushed between the parallel supports of a standard testing machine. Two identical components were tested of each design variant. The specimens were clamped in a test fixture for 10 mm along the top and bottom edges of the 200 mm high specimen (180 mm free vertical height). This test configuration simulated the constraints provided by the upper cabin floor and the lower outer subfloor shell. The vertical edges were not supported. Unsupported edges occur in many existing metal subfloors which have large circular cutouts 100 mm from the cruciform intersections.

## 2.2 Cruciform crush test results

### 2.2.1 Crushing behavior evaluation criteria

The crushing behavior and energy absorption performance of a collapsing structural element are evaluated by commonly used criteria. Fig. 3 summarizes the criteria used in the present investigation. A very important criterion for lightweight energy absorbing structures is the specific absorbed energy (Esp), i.e. the absorbed energy divided by the structural mass of the absorber or structure. Often only the crushed mass is taken into account. In the present work the total cruciform mass is used in calculating the specific energy. The total mass was used because the element did not show a clear crush front, making the mass of the crushed portion difficult to determine.

Another commonly used criterion is load uniformity which is the ratio of the peak failure load ( $F_{peak}$ ) to the average crush force level ( $F_{avg}$ ). The "ideal" absorber with a rectangularly shaped force-deflection curve has a load uniformity value of one. Higher values indicate unfavorably high peak loads. The inverse of the load uniformity is defined as the "crush force efficiency" A.E. and is typically used. With this criterion the "ideal" absorber has an efficiency of 100 percent and lower percentages indicate deteriorating performance.

Additionally, the initial element compression stiffness of the load-deflection response,  $K_{test}$ , is an important parameter for hybrid computer crash simulation programs. In these programs a crushable element such as a cruciform is modeled with a spring of stiffness,  $K_{test}$ .

### 2.2.2 Force-deflection characteristics and failure modes

The force-deflection curves of all tested cruciforms except the "improved design" element (HTP) have basically the same shape because of instabilities which initiated failure for all specimens. After an initial peak failure load, the crush force drops in most cases to a much lower value. The average crush force then remains almost constant or increases up to a stroke of about 125 mm. Fig. 4 shows the crushing characteristics of the aluminum single "notched" element (ALN1), the hybrid element with corrugated edge joints (HW) and the hybrid "improved design" element (HTP). The initial peak failure load and the initial stiffness ( $K_{test}$ ) of all tested designs are given in Fig. 5.

The aluminum cruciform with a single notch in the middle of the angle joint had better crushing and energy absorption characteristics than the multiple notch configuration. At low compression levels, instabilities of the baseline aluminum cruciform plate sections could be observed at the unclamped edges. However, the vertical plate junctions remained straight. With further increases in load the midsections buckled and started to fold and form plastic hinges. This folding was followed by fractures. The aluminum "notched corner" configurations started to fail and form plastic hinges at the notched areas.

Most composite cruciform elements showed an abrupt drop in load after the first failure as can be seen looking at the crushing characteristic of the corrugated edge joint CFC/AFC hybrid cruciform (HW), Fig. 4. However, the absolute energy absorption of the HW-element was already higher at 125 mm of stroke than the best aluminum configuration (ALN1). The CFC/AFC-hybrid element with the column-like midsection (HTP) showed outstanding crushing characteristics and energy absorption performance. This performance comes close to what is considered "ideal" for a subfloor element. The initial peak force was approximately 32 kN and the maximum force level of 39 kN was reached at a 90 mm deflection. After the trigger zone failed the element folded and cracked in a very regular fashion. This uniform crushing behavior was especially apparent at the column-like midsection. The undulations in the force-deflection curve indicate the progressive folding of the HTP-element. The absolute energy absorbed by the HTP-element was 2.3 times greater than that of the HW-composite cruciform.

The failure characteristics of the hybrid cruciforms were most similar to the aluminum elements on a macroscopic level. The hybrid cruciforms tended to fold like the aluminum, did not disintegrate, and provided post crush integrity because of the layers of AFC in the laminate as can be seen in Fig. 6. Pure CFC-cruciforms failed abruptly at the bottom of the intersection. Most of the CFC-element was completely destroyed at the crush front and showed no post crush integrity. However, the numerous local fractures and friction from fractured parts sliding resulted in the pure CFC-cruciform having a high energy absorption.

### 2.2.3 Energy absorption performance

The specific absorbed energy ( $E_{sp}$ ) and the absolute energy absorption ( $E_{sp}$ ) are shown in Fig. 7 where the results are averaged values of the two tests conducted. Also included in Fig. 7 are values of the element mass relative to that of the aluminum baseline element (100 percent). The highest  $E_{sp}$ -value of 14 kJ/kg and highest absolute energy

absorption of 2938 J were obtained with the hybrid HTP-element. The outstanding crushing characteristics and energy absorption of the hybrid HTP-element make it a preferred design variant even when the increase in manufacturing effort is considered. The single notched aluminum cruciform (AlN I) is a "minimum-modification" concept and is the best aluminum configuration with respect to specific energy (5 kJ/kg) and absolute energy absorption (1218 J). The pure carbon element also shows relatively high energy absorption (7 kJ/kg and 1230 J) and provides the highest weight savings (28 percent) compared to the aluminum baseline. However, the poor post-crush structural integrity of the pure carbon element must also be considered if this concept is used in a subfloor.

### 3. Sine wave beam subfloor elements

In vehicles designed to meet the requirements of MIL-STD-1290 A or ADS-36 approximately 40 percent of the crash related kinetic energy is absorbed by progressive crushing of the subfloor beam structure. Energy absorbing subfloor beams must be designed to perform the dual role of reacting the fuselage bending loads and progressively crushing in a crash. The U.S. Army and DLR have investigated sine-wave beam structures or the similar tangent circular ring segment beams quite extensively under crash and shear loading conditions (10 and 11). Other beam configurations such as sandwich beams or circular and rectangular tube integrally stiffened beams have also been considered. However, sine wave beam structures are the most efficient design concepts yet evaluated. These beams combine high load carrying capability and efficient energy absorption in the web direction with excellent structural post-crush integrity by using hybrid lamination techniques.

An experimental/analytical program was initiated to investigate systematically the structural response of sine wave beam sections. The approach includes basic research on the elastic and strength properties of woven composites (12) with the main emphasis on hybrids. Also, parametric studies on the shear/compression buckling behavior of sine wave beams were conducted (13). Finally, structural component testing was used for analysis validation and for determination of the energy absorption capability. Some of the structural component testing will be described in the following sub-sections.

#### 3.1 Energy absorption performance

Specific crushing stresses of various sine wave beam sections determined under quasi-static and dynamic crushing are shown in Fig. 8. The specific crushing stress is determined by dividing the average crush stress by the laminate's density. The specific crushing stresses in Fig. 8 are plotted against the CFC-volume fraction of the web laminate. Pure AFC-and CFC-beam webs and various AFC/CFC hybrid configurations were investigated. Hybridization was performed by either alternating pure AFC-and CFC-lamina in the stacking sequence (KCSIN) or by using intraply woven AF-/CF-fabric lamina. All dynamic drop tests were performed in the DLR drop tower at approximately 10 m/s initial impact velocity.

In Fig. 8 the dynamic specific crushing stresses were not consistently higher than the static stresses or vice versa. The phenomenon which caused these stress inconsistencies are related to failure modes which develop in each case. If the sine wave beam crushes in a controlled uniform manner, then the stresses will be higher than if

the specimen fails nonuniformly. The pure AFC-web elements (KSIN) had higher dynamic crushing stresses because of the development of a uniform local buckling (folding) failure mode for the dynamically tested specimen. For the hybrid elements (KCSIN, HSIN1) and the pure CFC-web element, the dynamic specific crushing stresses were much lower than the static stresses. The lower crushing stresses were caused mainly by irregular brittle fractures in the CFC-portions of the laminates. However, two hybrid elements (HSIN2 and HSIN3) had higher dynamic stresses because of a different failure mode. For these specimens, irregular local buckling and fracturing were observed during the quasi-static tests. During the dynamic tests, these same specimens failed progressively by a very efficient laminate bending mode. In this mode the CFC-portions of the laminate fractured completely and then embedded between a delaminated net of AF-rovings. The post-crush structural integrity was better for the specimens with the highest percentages of AFC as expected.

The energy absorption performance of composite sine wave beams is compared to equivalent aluminum structures in Fig. 9. The crush characteristics of an AFC/CFC-hybrid element (HSIN2) and an aluminum beam with trapezoidally corrugated web are compared. Although both beam webs have the same mass, the composite element absorbed twice the energy. However, the composite element has an undesirably high initial peak load. This problem will be discussed in the following section.

### 3.2 Influence of trigger mechanisms

The shape of the load-deflection curve from a crushing test is important in the crash response of a subfloor structure. The "untriggered" sine wave hybrid beam (Fig. 10) shows a static initial peak force of 48 kN, followed by an almost constant average crushing force level of about 20 kN. These values result in a crushing force efficiency of only 40 percent. When trigger slots are used in the bottom of the web, the initial peak load is reduced to 22 kN which is below the average crushing force level of approximately 23 kN for that particular test. The initial compression stiffness was not affected by the trigger slots. With the "triggered" configuration an almost ideal crushing force efficiency of about 100 percent is achieved. However, notch-type triggers must be treated very carefully, because they also severely reduce the beam's shear load carrying ability. Therefore, further research is needed to optimize practicable trigger mechanisms. Crushing initiators should preferably be embedded smoothly and uniformly in the laminate architecture.

## 4. Fuselage frame and floor sections

### 4.1 Experimental test specimens

The photographs in Fig. 11 show a section of a 1.83 m diameter circular frame, a close-up view of the Z-shaped cross section, and a splice plate used to join 90 degree frame segments. The frame cross section is 76 mm high, 57.2 mm wide, by approximately 2 mm thick. The frame was fabricated from a prepreg of five harness satin weave graphite fabric in a Hercules<sup>1</sup> epoxy matrix designated as 280-5H-AS4/3502. The

-----  
<sup>1</sup> Identification of commercial products and companies in this paper is used to describe the test materials. The identification of these commercial products does not constitute endorsement, expressed or implied, of such products by the U.S. Army, the DLR, or the publisher of these conference proceedings.

prepregs were draped over a lay-up tool into a quasi-isotropic lay-up.

The photograph in Fig. 12 shows both a skeleton and a skinned floor section specimen. Each floor section consists of three graphite-epoxy semi-circular frames, three aluminum floor beams, and fifteen pultruded graphite-epoxy stringers. The skinned specimen has a 1.6 mm thick graphite-epoxy skin bonded and riveted to the outside faces of the frames and stringers. Aluminum floor beams were used instead of graphite-epoxy beams to reduce specimen fabrication costs because the main objective of this investigation was to examine the response of the structural frame members below the floor. The cross-sectional dimensions of the graphite-epoxy Z-shaped frames used in the floor sections are identical to the dimensions of the individual frame specimens except for slightly thicker webs and flanges. The frames were manufactured in 90 degree segments and joined together with graphite-epoxy splice plates. These splice plates were located on both surfaces of the web and inside flange. Splice plates were not used on the outside flange (as they were used for the single frame specimens) to keep a smooth outer surface for bonding the skin to the frames and stringers.

Notches measuring 27.4 mm by 22.9 mm were machined into the frames of the floor sections for intersection with the pultruded stringers. The inside corners of the notches were machined to a 3.81 mm radius. The stringers were attached to the frames with riveted aluminum shear clips.

## 4.2 Results

### 4.2.1 Single frame static tests

A special purpose static test apparatus was used for testing the single frames. The specimen was sandwiched between a rear metal backstop and a front plexiglas shield. The plexiglas allowed visual observations and motion picture coverage of the frames. The purpose of the shield and backstop was to constrain deformations of the frame to the plane defined by the locus of frame cross-section centroidal points. The intent of constraining deformations was to limit twisting and out-of-plane bending of the frame. These modes were constrained to simulate the restraint of skin and stringer in an actual fuselage floor section. A steel loading bar 19 mm thick by 152 mm deep was attached to the graphite-epoxy frame. Loads were introduced into the frame through the steel bar using two hydraulic actuators. Motion of the hydraulic actuators was controlled by a servo valve and controller which kept the loading bar level during the tests.

The load-deflection response for the static test specimen and a schematic of the failure locations are shown in Fig. 13. The first peak of the load-deflection curve resulted when an instability occurred. The first failure location was 18 degrees to the left of the center contact point. This failure location is shown on the schematic. Failure occurred at the second peak on the load-deflection curve. Subsequent failure locations are also indicated in Fig. 13 by the peaks in the load-deflection curve. The frame buckled prior to the cross-sectional failure. The buckle was visible in photographs taken immediately before complete cross-sectional failure. The photographs indicate that the frame has twisted at the instability location. At a deflection of slightly more than 200 mm the load carried by the specimen dropped to zero and the test was terminated shortly thereafter.

The load-deflection curve given in Fig. 13 indicates that the specimen was carrying a load of 12 kN and had deflected 30 mm at the instability. The strain magnitudes before instability were not large enough to fail the graphite-epoxy material. But the strains were very high near the localized loss of stability and failure was initiated.

#### 4.2.2 Single frame dynamic tests

A summary of the dynamic tests is presented. A more complete discussion of the single frame drop tests is given in reference 6. Fig. 14 shows a graphite-epoxy frame after impacting a concrete floor at a 6 m/s velocity. A steel bar weighing 42.3 kg was used to represent floor mass. This specimen had three localized major fractures. The failure characteristics exhibited by this specimen were typical of other specimens. Motion picture films indicated that the first major fracture occurred near the impact point. Subsequent failures occurred 62 degrees to the left and right of the center impact point.

Filtered acceleration pulses at the frame-floor intersection are shown in Fig. 15 for two different test configurations. The average accelerations for these specimens were also determined from motion analysis of the high speed films taken of each specimen. These average accelerations substantiate the data shown in Fig. 15. The product of the peak acceleration and floor mass was used to estimate the maximum dynamic load exerted on the lower frame by the upper floor mass. Dynamic loads of 5.6 kN and 6.2 kN were determined for the frames. These load magnitudes are similar and occurred approximately 8 milliseconds (msecs) after impact. The calculated failure load from the dynamic test was approximately half of the measured static load and may have resulted from the filtering used to process the dynamic data. The unfiltered data had much higher acceleration peaks than the 60 Hz data presented in this paper. These higher accelerations may translate into higher actual loads being applied to the frame than calculated with the 60 Hz peak accelerations.

#### 4.2.3 Floor section static tests

##### 4.2.3.1 Skeleton section static test

A skeleton floor section was statically tested to failure. The specimen swayed sideward during the test. This swaying resulted because the aluminum shear clips used to join the frames and stringers yielded. The failure sequence is described as follows. Initially the frames remained vertical. Next, in addition to in-plane bending the frame deformed out-of-plane between points at the top and bottom where out-of-plane motion was restrained. This out-of-plane bending resulted in yielding of the aluminum shear clips and the combined out-of-plane and in-plane bending failed the specimen at critical notch locations. After the first fracture in each frame, the floor section was free to move axially and the frames shifted in the test machine. The aluminum shear clips prevented the composite Z-frames from twisting (no significant twisting was observed), but did allow bending out-of-plane which resulted in shearing of the frames and stringers.

The load-deflection response for the skeleton floor section test is shown in Fig. 16. The response of the floor section was almost linear up to a load of approximately 11.6 kN at which time the response flattened

out. This change in response is probably associated with yielding of the aluminum shear clips. After this yielding the floor section deformed laterally by bending out-of-plane. The maximum load carried by the specimen was approximately 16 kN. The load per frame was much lower than the single frame load because of the out-of-plane deformations and stress concentration at the notch. The test was stopped after approximately 300 mm of deformation because one frame was losing contact with the load platform.

#### 4.2.3.2 Skinned floor section static test

Because only one skinned floor section was manufactured, a nondestructive static test was conducted prior to a destructive impact test. The load-deflection response of the skinned floor specimen was linear after a slight initial increase in stiffness. This stiffening was probably caused by load redistribution among the 3 frames of the specimen because of small differences in the height of each frame. As expected, the skin kept the deformations planar and thus no out-of-plane bending or twisting were observed in this test. The vertical load-deflection stiffness was approximately 4 times greater than that of the skeleton specimen.

#### 4.2.4 Floor section dynamic tests

##### 4.2.4.1 Failure characteristics

The skeleton floor section is shown in Fig. 17 after a 6 m/s vertical impact onto a rigid concrete surface. The specimen's loading platform with 136 kg of attached mass has been raised to provide an unobstructed view of the frame failures. All three frames failed at the same five circumferential notch locations. Strain gage leads held some of the failed frame fragments together. The failure nearest the bottom contact point was located immediately to the right of the bottom splice plate.

A skinned specimen was also dynamically tested with a 6 m/s impact onto the same concrete surface. The same attached floor mass of 136 kg was used in this test. The damage to this specimen is much less than that of the skeleton specimen. Close inspection showed a total of nine fractures, three fractures occurring per frame. All nine fractures were located at notches. The fractures did not occur at the same circumferential location of each frame as occurred in the skeleton specimen. Some frames failed completely across the cross section but the skin held the two fractured ends together. Debonding of the frames from the skins did occur at some fracture locations.

##### 4.2.4.2 Acceleration response

Floor level acceleration pulses for the skinned and skeleton floor sections are shown in Fig. 18. The floor time histories presented are representative of the other accelerometer time histories. The acceleration data were filtered at 60 Hz. The peak acceleration of the skinned specimen is approximately twice that of the skeleton specimen. This increase in acceleration may be attributed to the greater measured static stiffness of the skinned floor section and its expected increased strength. Vertical crushing forces may be estimated from the product of the peak acceleration and the floor level mass. The floor section mass

was 136 kg which results in estimated vertical crushing forces of 53.4 kN for the skinned specimen and 26.7 kN for the skeleton specimen. The measured static structural crushing load for the skeleton specimen was 16 kN. Dynamically, the skeleton specimen might be expected to carry a larger load because of the failure mode observed in the static test. The specimens might not have enough time to bend out-of-plane which would result in a higher stiffness and strength. Statically, the skeleton specimen bent out-of-plane and swayed. This motion led to an early failure.

#### 4.2.5 Analysis and experimental correlation

##### 4.2.5.1 Analysis

The nonlinear dynamic structural finite-element code DYCAST (DYnamic Crash Analysis of STRuctures) (ref. 14) was used to model the frames for both static and dynamic loading cases. DYCAST was developed by Grumman Aerospace Corporation with partial support from the NASA-Langley Research Center.

Because of symmetry the DYCAST model consisted of a 90 degree segment of a single frame from the floor to the bottom contact point. Thirty-four straight beam elements gave converged results which accurately modeled the curved 180 degree frame. Isotropic laminate properties were used to calculate extensional and bending stiffnesses. Young's modulus was assumed to range from 48 to 55 GPa. A maximum strain failure criterion was used to specify the maximum compressive and tensile strains before failure. The material was assumed to be linear-elastic until failure. DYCAST accounts for partial failure of elements by monitoring the tensile and compressive strain magnitude at Gaussian integration points in the beam cross section. When the strain at an integration point exceeds the failure strain, the material properties (Young's modulus and shear modulus) at that integration point are set to zero. The element thus can carry partial load until the strain at all integration points exceed the failure strain. For a Z-cross section, a total of 9 Gaussian stress points are monitored. The boundary conditions and full field deformation constraints were found to be critical in modeling the frames. The non-symmetric Z-cross section tends to allow the frames to twist and move out of plane unless constrained.

##### 4.2.5.2 Static tests

The finite element code DYCAST was used to model a single frame. To compare the single frame test with the floor section (with three frames) static tests, the force applied experimentally to the floor sections was divided by three. Fig. 19 shows the comparison of the static test results of the single frame, skeleton floor section, and the skinned floor section versus DYCAST for small vertical displacements up to 18 mm. The DYCAST model used in each case was the same except for different constraints. For the skinned floor section simulation the model was constrained to remain inplane without twisting. For the skeleton floor section and single frame models, out-of-plane motion was allowed. For larger deflections the boundary conditions necessary to model the single frame behavior become very complicated. Initially the specimen can twist and deform out of plane. Later the specimen's deformations are restricted by the plexiglas and backstop.

#### 4.2.5.3 Dynamic tests

For dynamic DYCAST simulations, the implicit Newmark-beta time integrator was used with an initial time step of 0.00005 seconds. The floor loading for a single frame was represented by a lumped mass of approximately 42.3 kg and the impact velocity was 6 m/s. The single frame dynamic test attempted to restrict twist and out-of-plane bending in a similar fashion as the static test by sandwiching the frame between plexiglas and a rear backstop. However, as in the static tests the small clearance allows the frame to move out of plane initially. Fig. 20 shows the first 15 milliseconds of the experimental floor acceleration compared with two DYCAST predictions. In one analysis in-plane deformations were constrained to the plane of the frame, whereas in the other the frame was free to twist and bend out of plane. The agreement between the free DYCAST model and the single frame dynamic experiment is good for the initial peak. Later the agreement worsens because the plexiglas and backstop begin to provide support to the frame. The skeleton floor section acceleration pulse (Fig. 18) is also very similar to the single frame acceleration pulse. The constraint on the skeleton frames was similar to that experienced by the single frames. In all dynamic simulations, the failure strain was quite critical. A value of .0055 was used for these simulations. This value corresponds to the maximum value measured before an instability occurred for the single frame.

#### 5. Concluding remarks

Cruciform structural elements were crushed to determine their energy absorption capability to rotorcraft crash-type loads. Quasi-static compression tests were conducted on a series of aluminum and composite cruciform elements. This test series included various designs of "trigger-mechanisms" to reduce initial peak failure loads and to initiate stable crushing failure modes. All elements were designed to the same stiffness criteria as the keel beam and lateral bulkhead sections of the aluminum baseline element. Most of the cruciforms showed instability dominated failure modes which resulted from the specific structural shape of the elements. However, one CFC/AFC-hybrid element (HTP) with a column-like midsection behaved more like a well-designed tubular composite element. This hybrid cruciform crushed in an efficient controlled local buckling/brittle fracturing failure mode which resulted in an "ideal" subfloor crushing. To consider this element (HTP) for a subfloor design, the increased manufacturing effort required to fabricate must be mentioned. Hybridization techniques demonstrated their effectiveness with respect to post-crush structural integrity compared to pure CFC-elements. The inherent material properties of aluminum provided good post-crush integrity for cruciforms fabricated from this material. Multiple notched concepts with aluminum and composite cruciforms intended for peak failure load reduction did not work well and resulted in lower energy absorption performance. The absolute energy absorbed by some composite subfloor intersection elements was greater than that of the aluminum elements and the composite elements offered weight savings between 15 and 30 percent.

Sine wave beams are the most efficient design concepts yet evaluated for energy absorbing composite subfloor beams. Depending upon the laminate's configuration, specific crushing values between 20 and 60 kJ/kg were measured from the quasi-static and dynamic tests. These crushing values are within the range of very efficient tubular composite crush specimens. High values of specific crushing stress were obtained

for sine wave beam web laminates having a percentage between 30 and 40 percent AFC. These sine wave beam laminates also have good post crush integrity and acceptable shear buckling stiffness. A comparison between a corrugated aluminum web and a hybrid sine wave web of equal mass showed that the composite beam could absorb about twice the energy. Notch trigger mechanisms reduce the peak failure load effectively, but unfortunately also reduce the shear carrying capability of the beam. Further research is needed to develop optimized trigger mechanisms. These crushing initiators should be built into the laminate architecture so notching can be avoided.

The response and failure mechanisms of 1.83 m diameter graphite-epoxy frames and floor sections under crash-type loadings have been investigated. Using a building-block approach, the investigation began with single frames and progressed to a skinned floor section. Single circular frames with a Z-cross section were tested to examine the structural component thought to be the major contributor to the crashworthy response. To enable comparison of single frame tests with the complete floor section tests, the single frames had to be supported in a similar configuration as frames in the floor sections. This condition required that the single frames be sandwiched between front and rear fences to keep deformations of the frame planar. Analysis using the finite-element program DYCAST was useful in determining the effects of various boundary conditions (planar, out-of-plane bending, twisting, etc.) on the stiffness of the frames. The experimental set up for the single frame tests was not entirely successful in preventing out-of-plane bending and twisting of the frames.

The single frame failure was initiated by a loss of stability in both static and dynamic tests. The single frames and floor sections failed at discrete, widely spaced locations without absorbing much energy. The skeleton (no skin) floor specimen had approximately the same vertical crushing stiffness as the single frames, but failed at a much lower load per frame. It appears that the failure mechanism for the skeleton floor sections was different than that of the single frames. The skeleton floor sections experienced extensive out-of-plane bending in addition to in-plane bending. These specimens failed at notches without signs of local instabilities preceding these failures. The notches caused stress concentrations as well as reducing net cross-sectional area and stiffness of the frames. The stresses at the notches from the combined in-plane and out-of-plane bending caused failure to initiate at the notches at much lower strain values than those causing the instability problems. Addition of a skin to the floor section prevented the frames from bending out of plane. This constraint resulted in a four-fold increase in the vertical stiffness. It also resulted in a two-fold increase in the floor level accelerations for the impact tests. Unlike the skeleton floor section, the skinned floor section retained much of its structural integrity after the impact test.

From all single frame and floor section tests, much information was generated which would be helpful in developing simple, inexpensive, and valid test techniques for evaluating the impact resistant potential of other structural components. Shortcomings of proposed composite skin-stringer designs were discovered and the findings of this research will be useful for future investigations.

Several projects will serve as focal points for future cooperative activities. These projects include development of composite coherent collapsible frames, continued crash-resistant subfloor design studies, and improved analytical approaches. Improved analytical techniques are needed for prediction of energy absorption and dynamic response of composite materials and structures.

6. References

- 1) MIL-STD-1290 A (AV), Military Standard Light Fixed and Rotary-Wing Aircraft Crash Resistance, 26 September 1988.
- 2) ADS-36, Aeronautical Design Standard Rotary Wing Aircraft Crash Resistance, 1 May 1987.
- 3) G.L. Farley, Energy Absorption of Composite Materials, Journal of Composite Materials, Vol. 17, May 1983.
- 4) C. Kindervater, H. Georgi, and U. Körber, Crashworthy Design of Aircraft Subfloor Structural Components, 66th AGARD Structures and Materials Panel - Specialists' Meeting on Energy Absorption of Aircraft Structures as an Aspect of Crashworthiness, Luxemburg 1-6 May 1988, AGARD-CP-443.
- 5) D. W. Lowry, N.E. Krebs, and A.L. Dobyms, Design, Fabrication and Test of Composite Curved Frames for Helicopter Fuselage Structure, NASA CR-172438, October 1984.
- 6) R.L. Boitnott, E.L. Fasanella, L.E. Calton, and H.D. Carden, Impact Response of Composite Fuselage Frames, SAE Technical Paper 871009, April 1987.
- 7) R.L. Boitnott, and E.L. Fasanella, Impact Evaluation of Composite Floor Sections, SAE Technical Paper 891018, April 1989.
- 8) W.G. Hienstorfer, Crashsimulationsrechnungen und Bauteilidealisierung für einen Luftfahrzeugunterboden, Zeitschrift für Flugwissenschaften und Weltraumforschung, Band 11, Juli-Oktober 1987, Heft 4/5.
- 9) C. Kindervater, Energy Absorption Qualities of Fibre Reinforced Plastic Tubes, Proceedings of AHS National Specialist's Meeting on Composite Structures, Philadelphia, March 1983.

- 10) C. Kindervater, and D.C. Bannerman, Crashworthiness Investigations of Composite Aircraft Subfloor Beam Sections, Proceedings of International Conference on Structural Impact and Crashworthiness, Imperial College, London July 1984.
- 11) G.L. Farley, Crash Energy Absorbing Subfloor Beam Structures, Journal of the American Helicopter Society, October 1987.
- 12) W.G. Hienstorfer, Die "Soft Mosaic Theory" - eine Methode zur Bestimmung der Elastischen Kenngrößen und des Festigkeitsverhaltens von Gewebelaminaten, DGLR Jahrestagung, Darmstadt, 21-23 September 1988.
- 13) M. Läßle, Schubtragverhalten von FVW-Wellstegen - Analytische Untersuchung mit Hilfe der FE-Methode, DGLR Jahrestagung, Darmstadt, 21-23 September 1988.
- 14) A.B. Pifko, R. Winter, and P.L. Ogilvie, DYCAST - A Finite Element Program for the Crash Analysis of Structures, NASA Contractor Report 4040, January 1987.

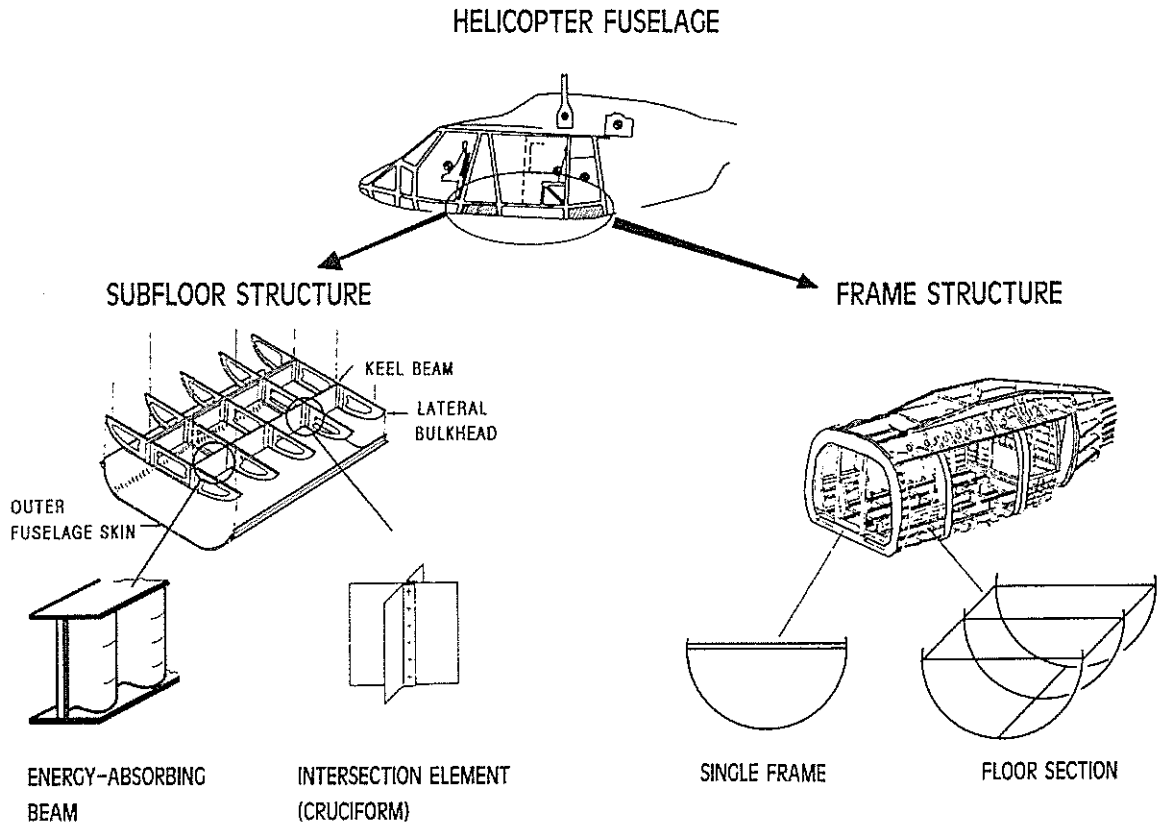


Fig. 1 - Examination of generic composite structures under vertical crash loading.

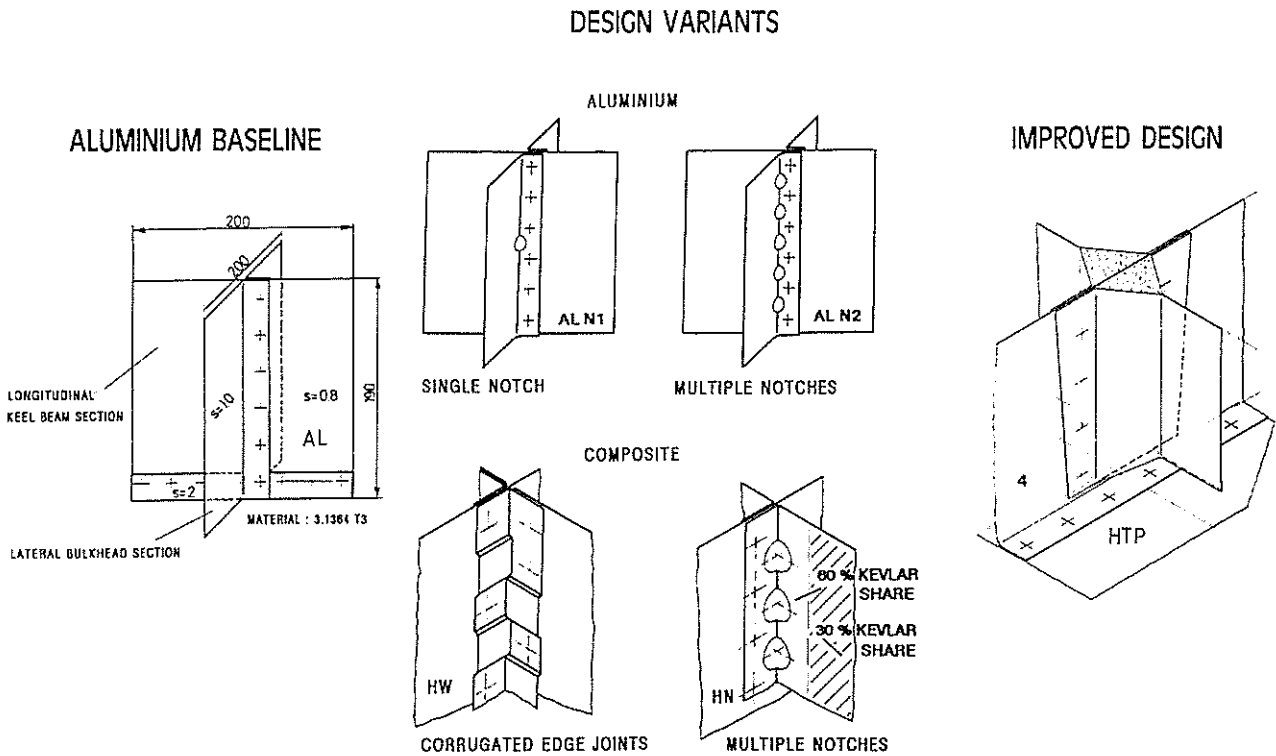
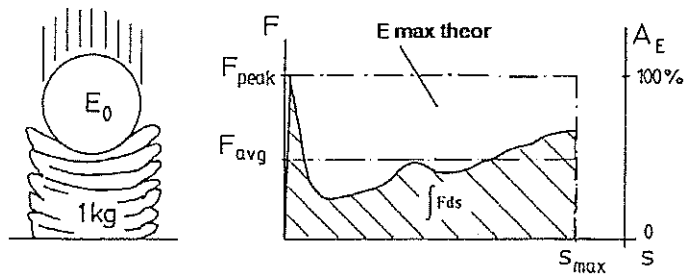


Fig. 2 - Structural cruciform design variants.



MASS SPECIFIC ABSORBED ENERGY :

$$E_{sp} = \frac{E_{abs}}{m} \quad [kJ/kg] \quad \text{with} \quad E_{abs} = \int_s F(s) ds$$

CRUSH FORCE EFFICIENCY :

$$A_E = \frac{F_{avg}}{F_{peak}} = \frac{E_{abs}}{E_{max theor}} \cdot 100 \quad [ \% ]$$

INITIAL COMPRESSION STIFFNESS :

$$K_{Test} = \frac{\Delta F_{peak}}{\Delta S_{peak}} = \frac{F(0.8 F_{peak}) - F(0.3 F_{peak})}{S(0.8 F_{peak}) - S(0.3 F_{peak})}$$

Fig. 3 - Definition of terms and crush behavior evaluation criteria.

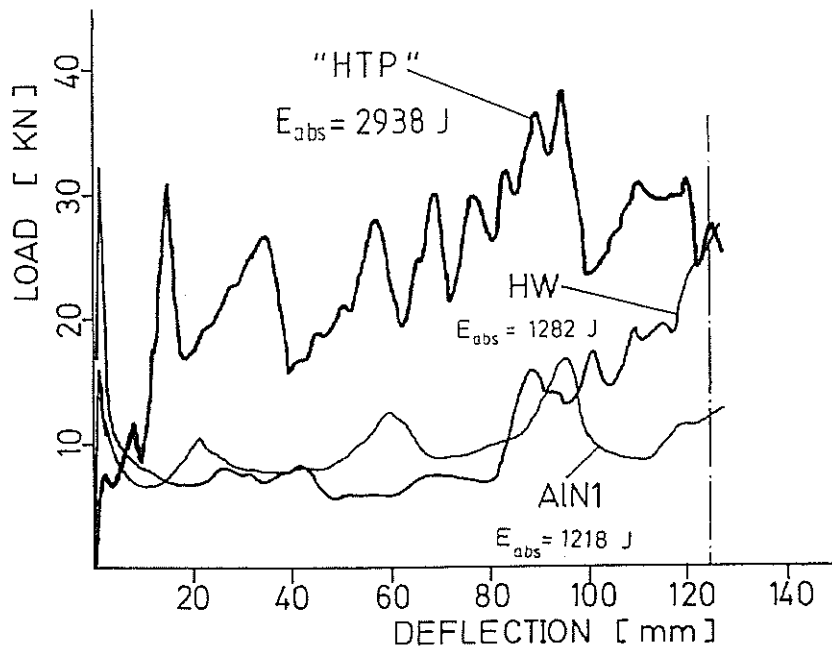


Fig. 4 - Crushing characteristics of cruciform elements.

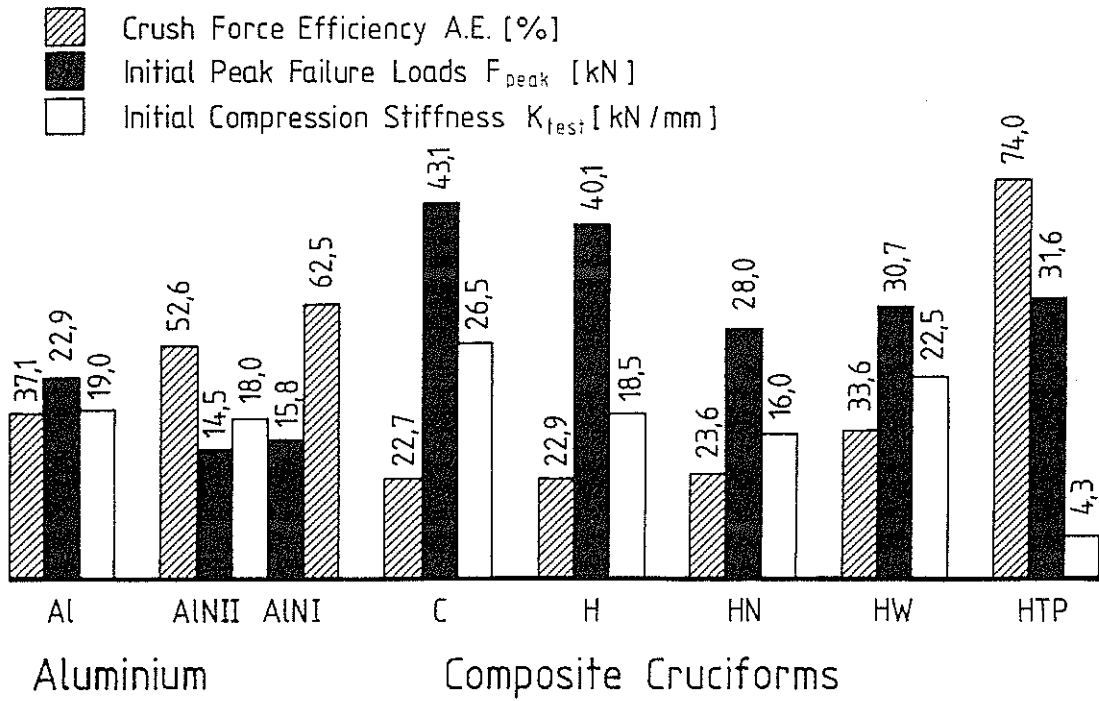


Fig. 5 - Crushing-characteristic cruciform parameters.

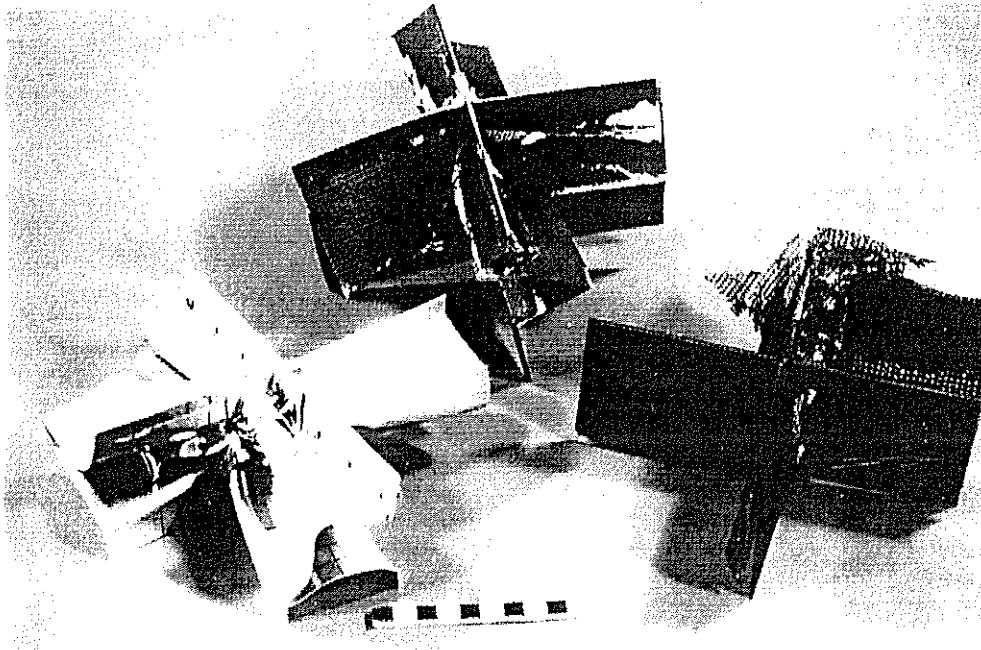


Fig. 6 - Cruciform element failure modes.

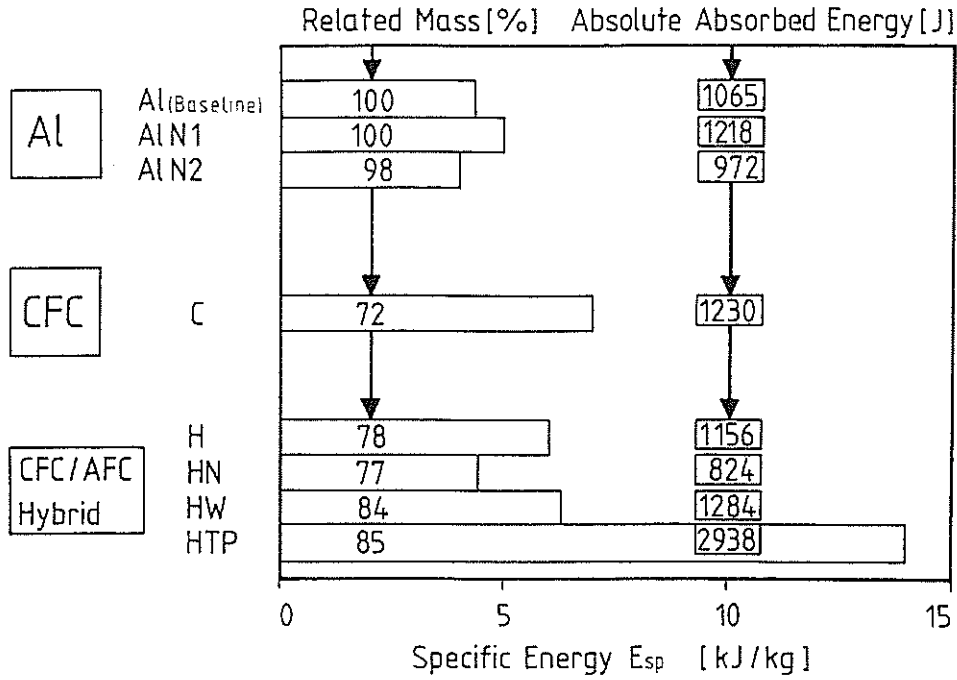


Fig. 7 - Energy absorption performance of cruciform elements.

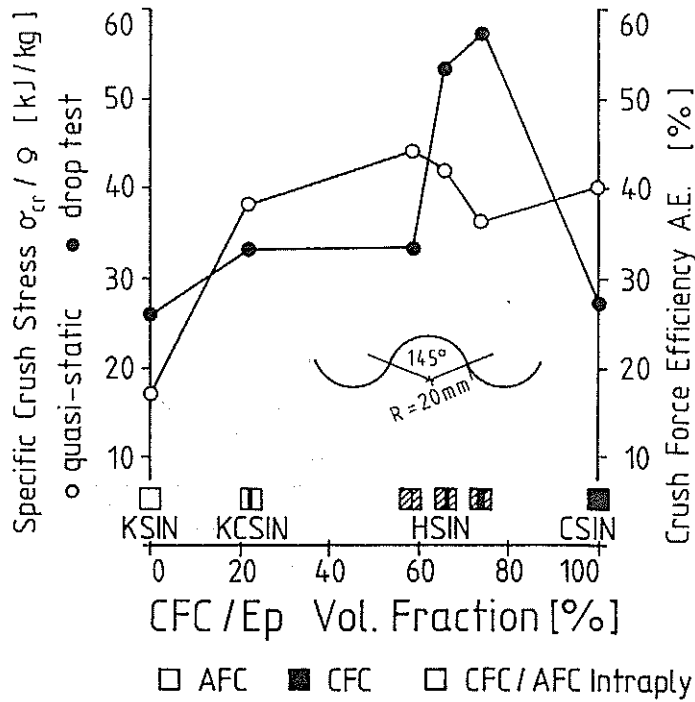


Fig. 8 - Specific crushing stress of sine wave beam sections.

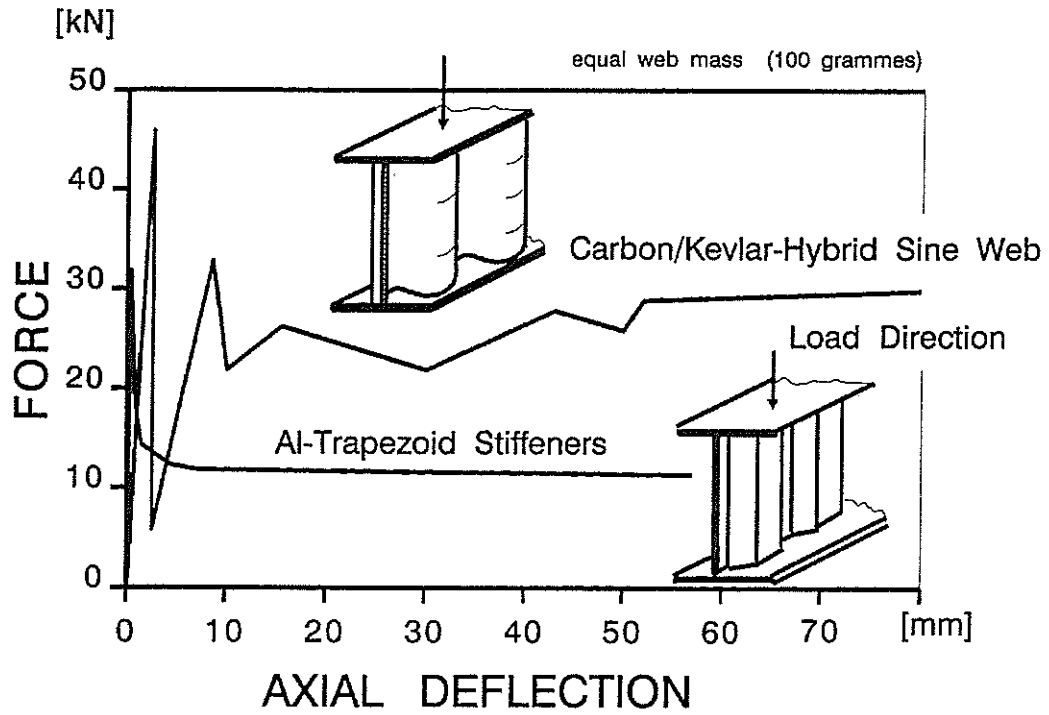


Fig. 9 - Crushing characteristics of composite sine wave beam and aluminum corrugated beam web.

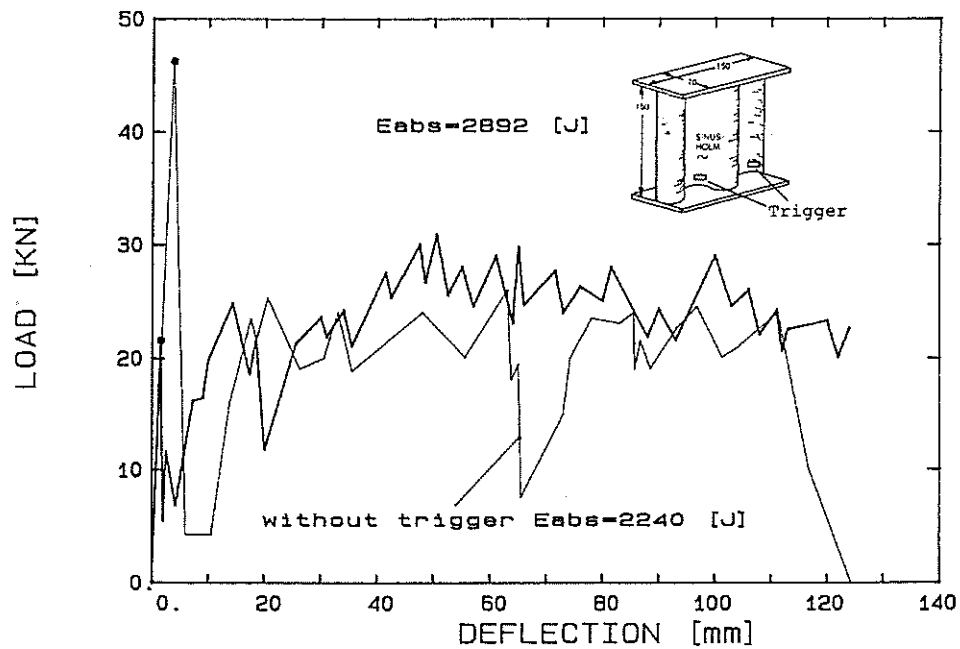


Fig. 10- Influence of trigger mechanism on crushing of sine wave beam webs.

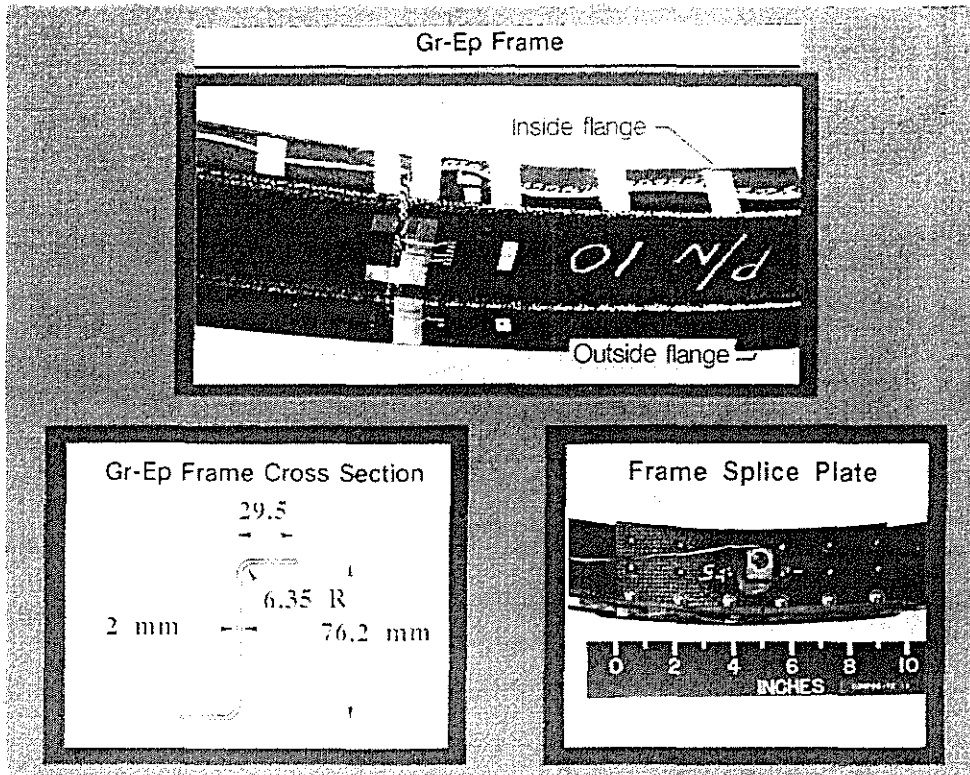


Fig. 11- Close-up view of graphite-epoxy Z-frame and splice plates. Nominal cross sectional dimensions of frame given.

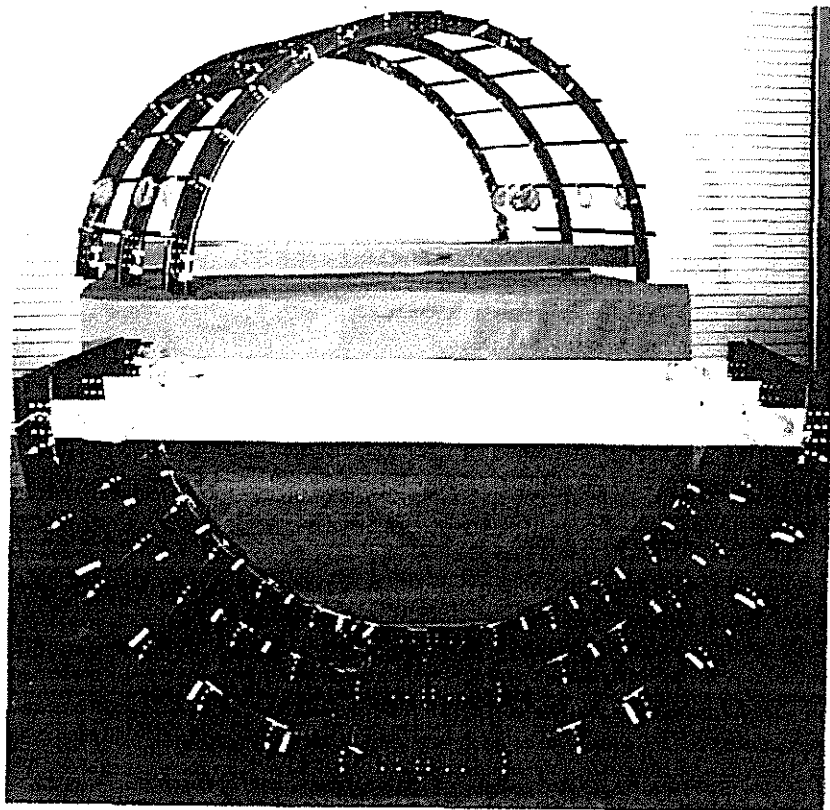


Fig. 12- Skeleton and skinned graphite-epoxy floor sections.

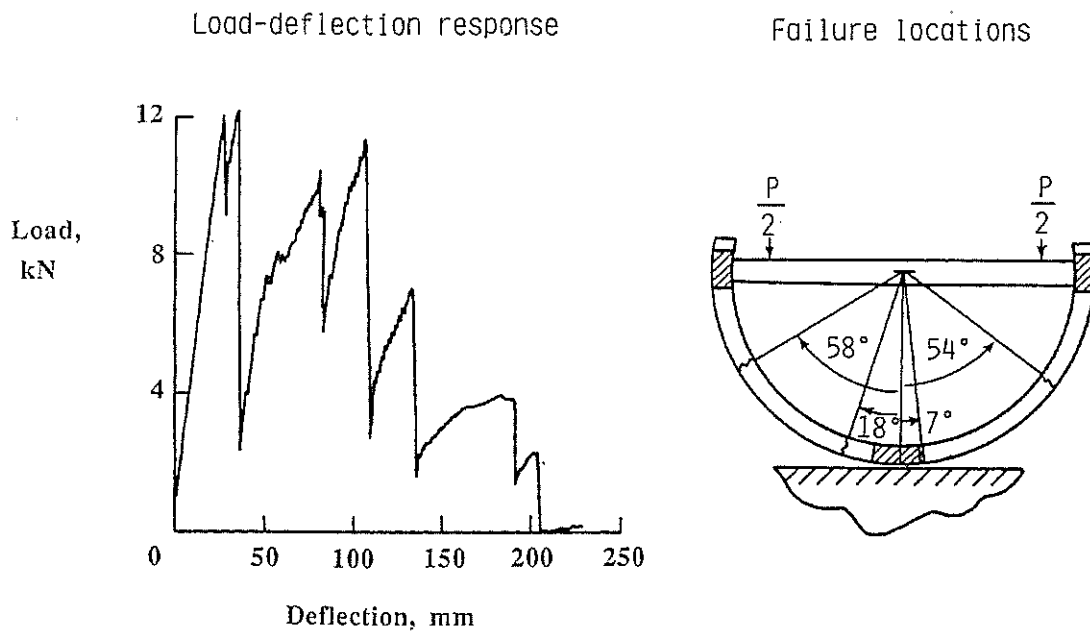


Fig. 13- Frame static test results.

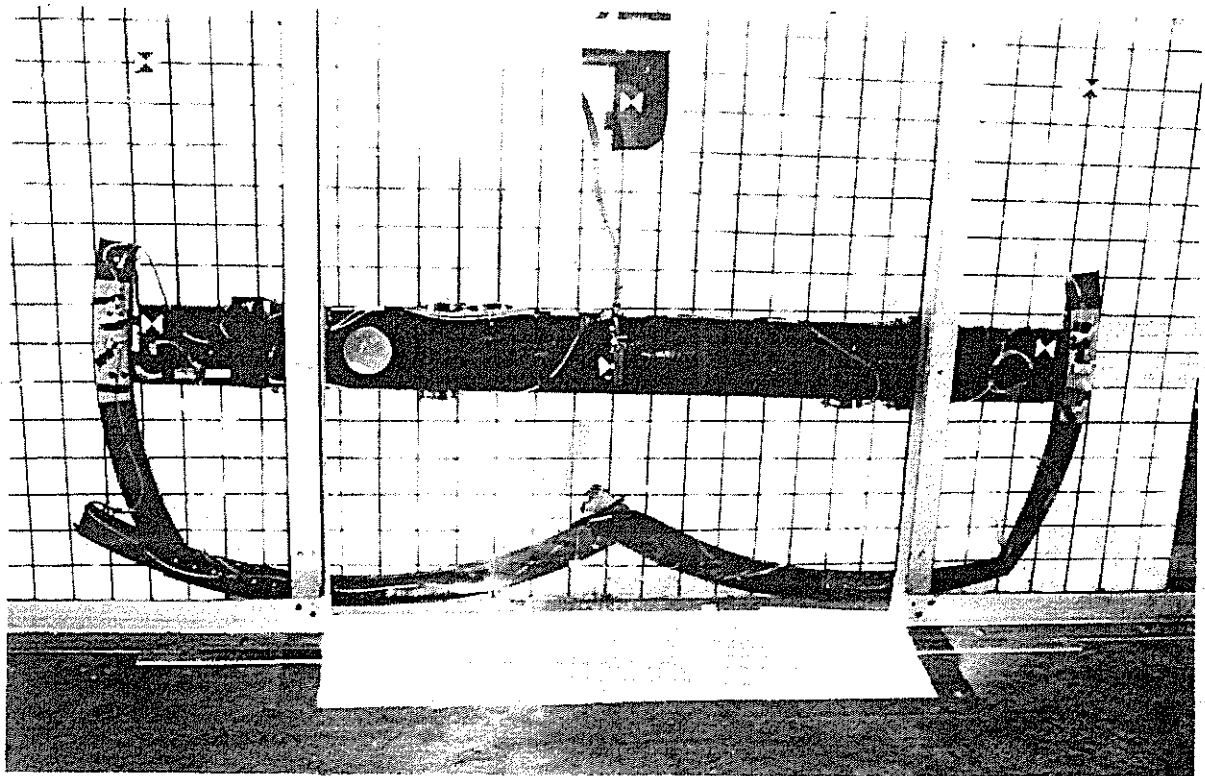


Fig. 14- Frame 5 after a 6 m/s impact test.

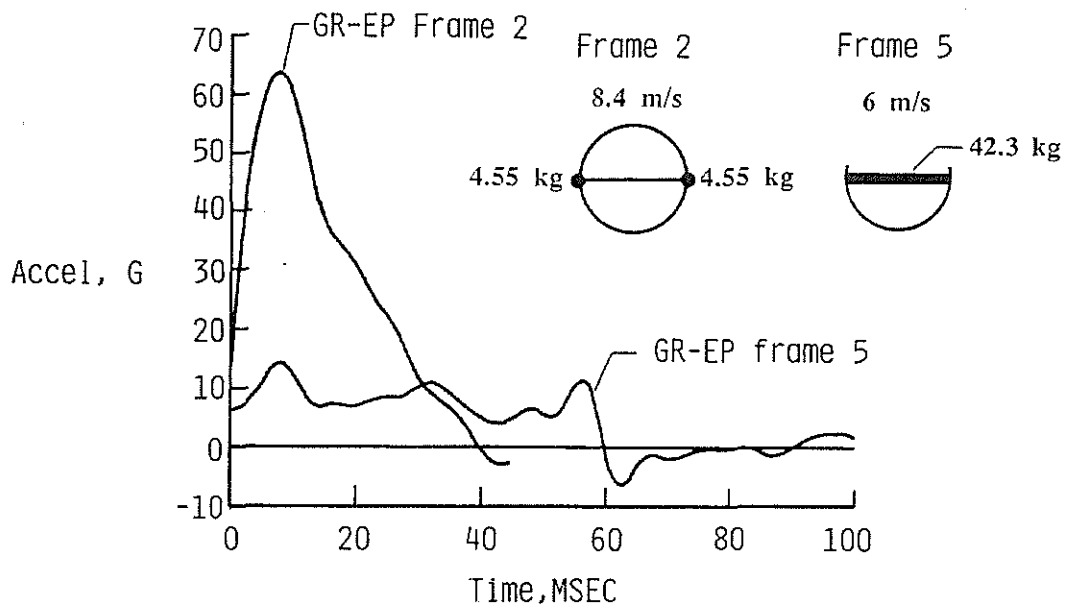


Fig. 15- Floor level acceleration pulses for two frames.

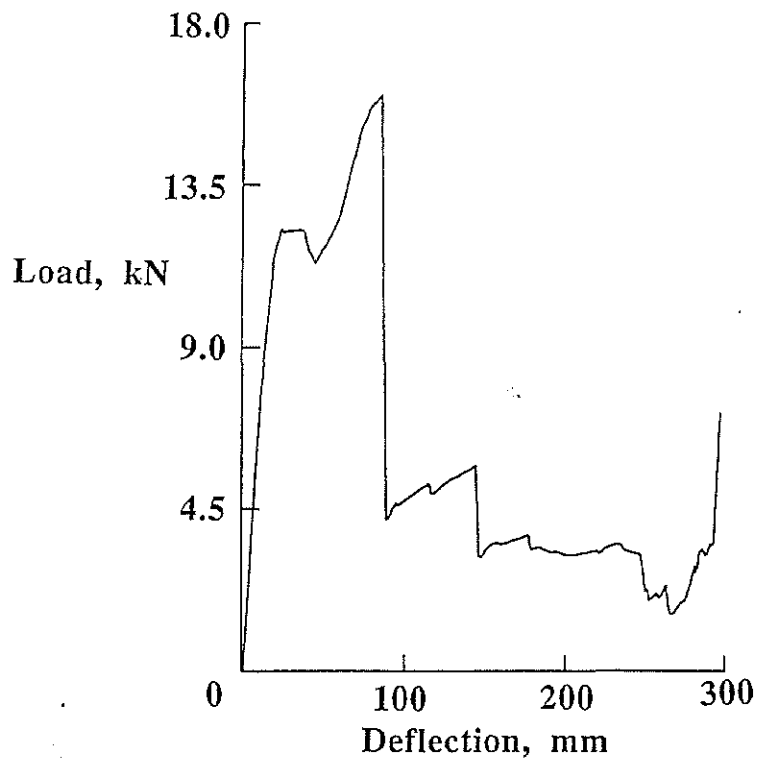


Fig. 16- Load-deflection response for static skeleton test.

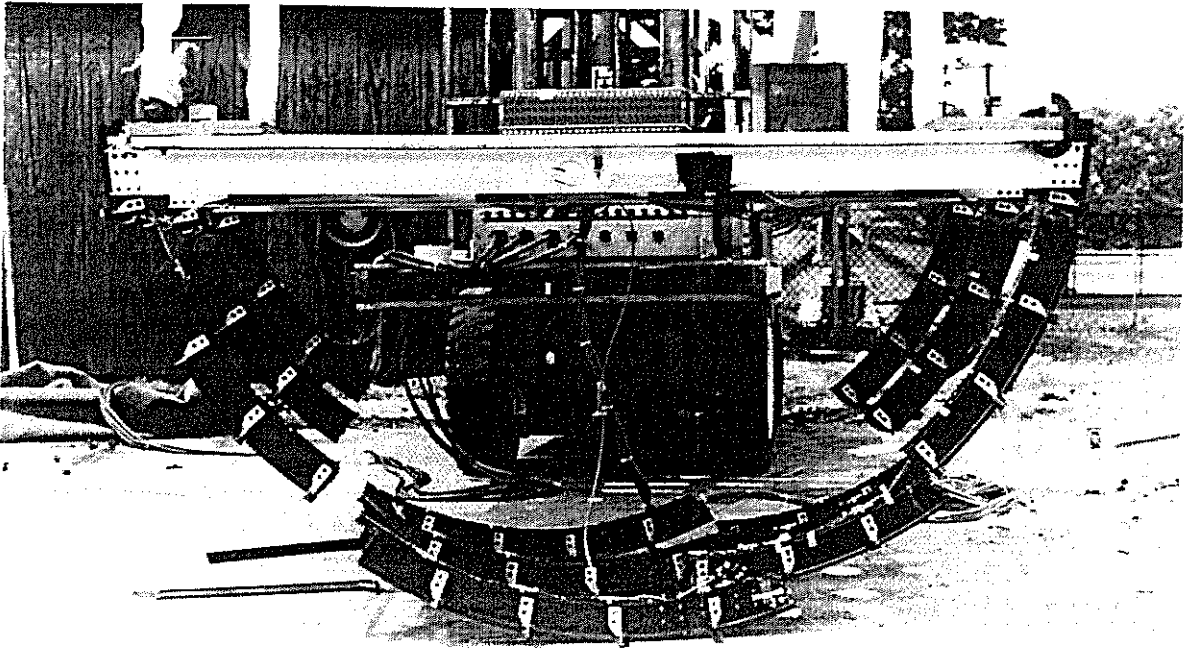


Fig. 17- Skeleton floor section after 6 m/s impact.

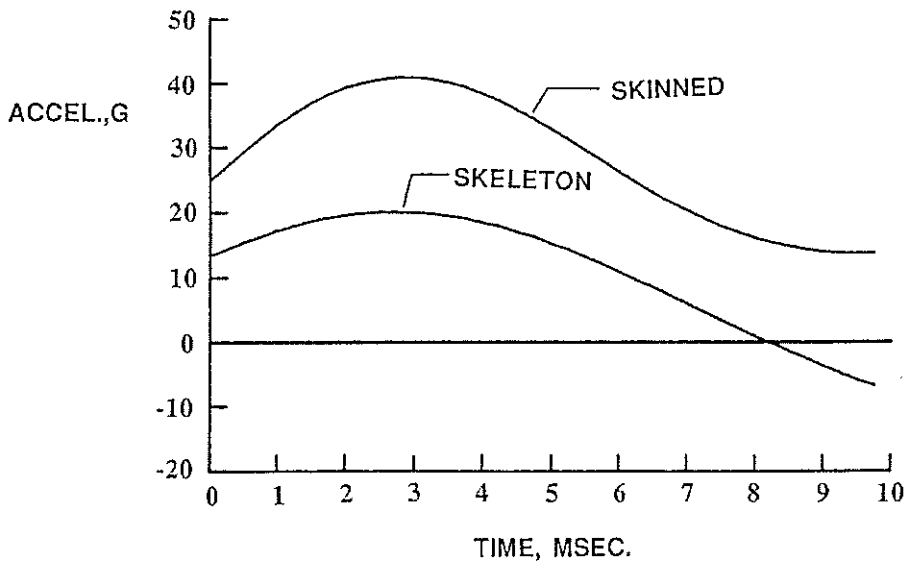


Fig. 18- Floor level acceleration pulses for skinned and skeleton floor sections. Accelerations were filtered with a 60 Hz digital filter.

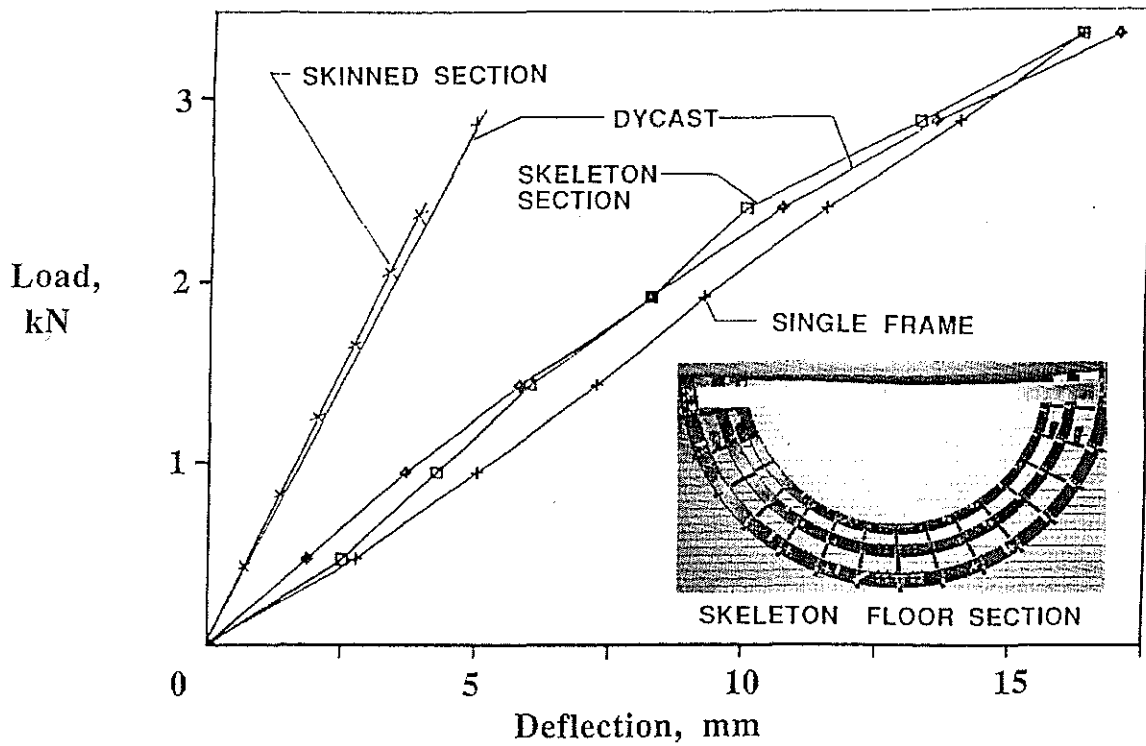


Fig. 19 - Load-deflection response from experiment and DYCAST analyses for single frame, skeleton floor section, and skinned floor section.

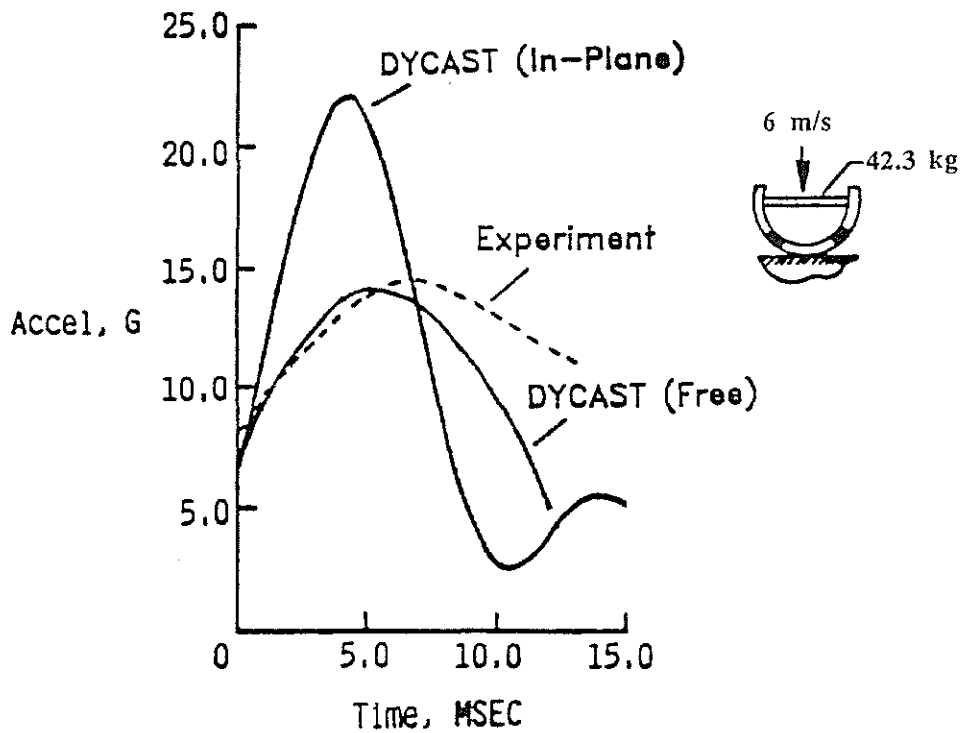


Fig. 20 - Impact response from experiment and DYCAST analyses for single frame. Two types of restraint were applied to the DYCAST model.